Catalysis Science & Technology

ROYAL SOCIETY OF CHEMISTRY

PAPER

View Article Online
View Journal | View Issue

Cite this: *Catal. Sci. Technol.*, 2025, **15**, 1028

Higher BTEX aromatic yield from ethanol over desilicated H,Zn-[Al]ZSM-5 catalysts†

Daniel Dittmann, Alime Ileri, Dennis Strassheim and Michael Dyballa *

The amount of BTEX aromatics obtained from the conversion of ethanol (ETA) is increased by combining ZSM-5 catalysts having optimum acidity with desilication and zinc ion exchange. Zinc leads to preferred dehydrogenation instead of hydrogen transfer. It decreases the share of paraffin products and increases BTEX contents (up to S_{BTEX} = 50%) at the cost of lifetime. The latter can be increased *via* desilication. An ethylene feed increases lifetime and BTEX production as result of oxygenate absence. Combination of improvements resulted in a C_2 conversion capacity of 206 g g^{-1} and a total yield of BTEX aromatics of 31.6 g g^{-1}, which is about a factor of 2–3 times better than the respective values found for microporous, mesoporous, or microporous Zn-exchanged materials. *In situ* UV/vis spectra reveal that desilicated samples coke significantly slower than microporous samples, whereas Zn exchange supports the formation of coke. Thus, by a clever combination of suitable post-modifications, a significantly higher BTEX production from the primary source ethanol can be achieved.

Received 3rd September 2024,
Accepted 18th December 2024

DOI: 10.1039/d4cy01062k

rsc.li/catalysis

1. Introduction

The workhorse of the large-scale chemical industry is heterogeneous catalysis. To boost the efficiency, porous inorganic solids such as zeolites are applied as catalysts or supports owing to their unique shape selectivity in chemical reactions.[1–3] However, further developments in this field are required to achieve the intended changes in resource basis and product chains. In particular, a CO_2-neutral basis for the chemical industry has to be developed, preferentially based on the current available production capacities. Ethanol has been identified as a perfectly suited resource owing to its easy availability, well-researched properties, and current availability in large scale volumes.[4] In future, ethanol may be applied as a resource for synthesizing aromatics, such as jet fuels, that require a high content of aromatics.[5] It is also of interest in synthetic chemistry. In particular, benzene, toluene, ethylbenzene, and xylenes (BTEX) are important. However, they are difficult to be synthesized from renewable sources. Thus, the conversion of ethanol into aromatics (ETA) over zeolites is now more intensively researched.

In their foundational work on alcohol conversion over ZSM-5 zeolites, Derouane *et al.*[6] reported a similarity between the conversion of methanol and ethanol. The conversion of methanol (C_1 unit) runs over reactive surface methoxy species (SMS) at Brønsted acid sites (BAS) inside ZSM-5 pores.[7,8] Conversely, methoxys on weakly acidic OH-groups under similar conditions are not reactive in the methylation reaction.[9] Multiple groups have likewise identified surface ethoxy species (SES) on the surface of ZSM-5 zeolites during ethanol (C_2 unit) conversion.[10–14] However, in contrast to C_1 methanol, C_2 ethanol already contains a C–C bond. Furthermore, the olefin-based cycle intrinsic to MTO is widely absent for ethanol conversion.[12] Ethanol is dehydrated to ethylene at comparably low temperature and acid site strength, and even γ-Al_2O_3 is catalytically active.[15,16] Thus, its dehydration into ethylene over ZSM-5 is an established route that will be replaced in the future by a route over coke-resistant heteropoly acids.[17,18] Ethanol dehydration occurs through a mono- or bimolecular mechanism over diethyl ether and reactive triethyloxonium ions as intermediates.[13,19] There are hints that the BAS location, in particular the presence of single *vs.* paired BAS, determines the preferred mechanism.[14] Ethanol dehydration is thus a necessary pre-reaction in the conversion of ethanol into hydrocarbons, which as per definition, makes ethylene and water the primary products of the ETA conversion.

The subsequent conversion of ethylene into hydrocarbons is a mechanistically separated reaction. It involves the homologation, cracking, and aromatization of the intermediate ethylene.[20,21] Most aromatics contain even numbers of hydrocarbons, and the homologation reaction is the predominant step for the final product distribution.[12] The

Institute of Technical Chemistry, University of Stuttgart, Pfaffenwaldring 55, 70569 Stuttgart, Germany. E-mail: michael.dyballa@itc.uni-stuttgart.de

† Electronic supplementary information (ESI) available. See DOI: https://doi.org/10.1039/d4cy01062k

desired products, aromatics, are coke precursors and cause a strong deactivation of the ETA catalyst. Hydrocarbons with uneven carbon numbers are explained by cracking, whereby surface methoxy species (SMS) can be formed.[12] Although the initial feed composition is quite different, methanol and ethanol routes to hydrocarbons involve a comparably complex reaction network. Main difference is a faster growth of hydrocarbons due to the oligomerization of the C_2 units. It is thus clear that the reaction conditions and catalysts need to be optimized independently for the respective feeds. For ETA conversion, properly adjusted ethanol partial pressure, WHSV, and temperature, as well as surface acidity are prerequisite for high aromatic contents.[22,23] As the main deactivation pathway is coking, strategies to counter fast coking were developed. Co-fed water can attenuate the deactivation due to coke; in parallel, a properly adjusted stoichiometry between water and ethanol can optimize the selectivity to aromatics.[22,24,25] The reason for this ability is that water and the alcohols show different tendencies to adsorb at surface groups like acid sites or cations,[26,27] since both compete for the catalytically active BAS on the zeolite.[28,29] An oxygen-optimized feed of diethyl ether or an oxygen-free ethylene feed can enhance BTEX production and lifetime.[25] A similar picture has been observed in methanol conversion, where dimethyl ether instead of methanol leads to increases in the lifetime by avoiding the formation of deactivating oxygenates like formaldehyde.[30–32]

Besides the feed, a typical strategy to increase the selectivity in methanol conversion involved engineering the density and strength of the catalyst, in particular the catalytically active BAS.[33–37] Comparable effects of BAS density on the product distribution and lifetime are found in the case of the conversion of ethanol over ZSM-5.[23,25,38] The BAS density on the external surface and within mesopores did not systematically affect the reaction due to the low external BAS densities (usually <0.05 mmol g^{-1}).[25,38] Larger zeolite crystals lead to a faster deactivation in the ethanol conversion without changes in the product distribution.[39] Nanosized (~30 nm) crystals were reported to have a higher yield of aromatics, but differed strongly from their μm-range counterparts in terms of acidity, porosity, and optimum temperatures for the catalytic testing.[40] Fast coking is caused by a slow diffusion of coke precursors out of the pores and pore clogging; therefore, hierarchical catalysts show potential in attenuating the deactivation.[41] Desilicated ZSM-5 catalysts have previously been applied by multiple groups to enhance the lifetime in the ETA conversion.[38,42–44] Synthesis of desilicated ZSM-5 catalysts involves subsequent treatments in base and acid solutions.[45–47] It should be noted that changing the alkaline agent from NaOH to KOH can increase the amount of introduced mesopores in high-silica 10-MR zeolites.[38,48]

The modification of H-ZSM-5 with nickel attenuates the deactivation.[24] Zinc is another promising and less harmful heteroatom. Its outstanding dehydrogenation activity was demonstrated in the methanol conversion, propane dehydrogenation, and in the dehydrogenation of ethanol to acetaldehyde.[49–51] Publications on MTO show that a dehydrogenation pathway is opened by the introduced Zn. It releases elemental hydrogen, while BAS-catalyzed paths require transfer of hydrogen to olefins, thereby generating paraffins in stoichiometric ratios.[50,52] Zn-cations exhibit a similar behavior when converting alkanes or alkenes.[53–55] These Zn-cations are octahedrally coordinated in ZSM-5 by water in the hydrate state, while some $Zn(OH)^+$ is formed in high loadings, if the binding BAS density or location allows no compensation of the two-fold positive charge of the Zn^{2+} cations.[56] It is noteworthy that zinc can insert into the framework at silanol nests if highly defective structures like dealuminated BEA zeolites are applied as hosts.[57] Steamed Zn–ZSM-5 was reported to exhibit better stability than the microporous counterpart.[58] Saha and Sivasanker[59] investigated Zn-loaded ZSM-5 catalysts in the ETA conversion, and reported increased amounts of aromatics and lifetimes without accounting for changes in the BAS density. Thus, until now, the effect of Zn-exchange on hydrogen transfer was not separated from the changes of reaction mechanism induced by the altered BAS density upon ion exchange. Furthermore, the ETA conversion was not measured under optimal reaction conditions. Thus, it is unclear how strong the ETA conversion benefits from bifunctional ZSM-5 zeolites that contain active Zn cations.

In this work, several optimizations for the ETA conversion over Zn–ZSM-5 catalysts are combined to enhance the selectivity to BTEX aromatics and the lifetime. Therefore, industrial ZSM-5 catalysts are first compared to their desilicated counterparts. In a second step, these parents are exchanged with Zn-cations to enhance the selectivity to BTEX aromatics. In a last step, the water content of the feed is also optimized. Multiple post-modifications are balanced and the respective optima are identified, which demonstrates how a clever combination of dedicated post-modifications results in significant performance improvement.

2. Experimental

2.1. Material preparation

Herein, all applied materials were synthesized from parent H–ZSM-5 zeolites CBV 2314 and CBV 5524G (Zeolyst Inc., USA). Before further use, the samples were calcined (6.5 h at 813 K in synthetic air) and exchanged with ammonium nitrate (Merck, Germany). Typically, 1 g of the ZSM-5 material was stirred in 10 mL of a 0.1 M ammonium nitrate solution at 353 K for 3 h. Then, it was subsequently filtered off and washed until nitrate-free with demineralized water. The ammonium-exchanged materials that were desilicated were treated according to Dittmann *et al.*,[38] applying the treatments depicted in Table 1. Briefly, 4 g of the ammonium-exchanged parent was added to 120 mL aqueous sodium hydroxide at the reaction temperature of 338 K, and stirred for 15 or 30 min. The reaction was quenched in an ice bath, and the solid removed by centrifugation, washed and

Table 1 Treatment conditions for synthesis of mesoporous ZSM-5

Sample	Base treatment	Acid treatment	Yield from parent [%]
D11	0.8 M NaOH 30 min	0.5 M HCl 6 h	69.7
D29	0.4 M NaOH 15 min	0.5 M HCl 6 h	80.6

dried. Afterwards, the solid was treated for 6 h at 338 K with 0.5 M aqueous hydrochloric acid (100 mL g^{-1} ZSM-5) to remove potential deposits. The reaction was again quenched, and the solid was removed by centrifugation, washed and dried. All materials were loaded with zinc *via* multiple ion exchanges, as indicated in Table S1 in the ESI.† For ion exchange, 5 g of the parent material (either microporous or desilicated ZSM-5) was stirred in 25 mL of an aqueous zinc nitrate (Merck, Germany) solution (35 g L^{-1}) for 1 h at 353 K. Afterwards, the solid was filtered off, washed with demineralized water, and dried at 383 K before it was calcined at 723 K for 2 h.

2.2. Characterization

The chemical composition of the materials was determined with inductively coupled plasma optical emission spectrometry (ICP-OES) at an IRIS Advantage instrument. X-ray powder diffraction on a Bruker D8 diffractometer instrument equipped with an X-ray tube for Cu Kα radiation (λ = 1.5418 Å) was conducted to elucidate the crystalline structure in a 2θ range of 4–50°. The inner surface and pore volumes were calculated from nitrogen physisorption measurements conducted on a Quantachrome Autosorb 3B at 77 K. Beforehand, the samples were activated at 623 K for 16 h. The inner surface was calculated by applying the Brunauer–Emmett–Teller (BET) equation, and the *V*–*t*-method (deBoer) was used to determine the micropore volume. The mesopore volume was calculated as the difference between the micropore and total pore volume, and the latter was determined at p/p_0 = 0.99. ^{1}H, ^{27}Al, and ^{31}P MAS NMR spectroscopy was performed on a Bruker Avance III WB spectrometer with a magnetic field of 9.4 T. The resonance frequencies for the ^{1}H, ^{27}Al, and ^{31}P nuclei were 400.1, 104.2, and 161.9 MHz, respectively. For measurements on ^{1}H and ^{31}P, an excitation pulse of π/2 was applied. For ^{27}Al, an excitation pulse of π/8 was applied. For ^{1}H MAS NMR measurements, the sample was previously activated for 12 h at 723 K (heating rate 1 K min^{-1}) and $p < 10^{-2}$ mbar. For ^{27}Al MAS NMR measurements, the samples were fully hydrated. Spinning rates for the 4 mm rotor were 8 kHz for ^{1}H and ^{27}Al and 10 kHz for ^{31}P, respectively. The latter was measured using high-power proton decoupling (HPDEC). For ^{1}H and ^{31}P measurements, the repetition time was set to 20 s. For ^{27}Al measurements, the repetition time was set to 0.5 s. Acid site densities were calculated after ammonia loading, as described elsewhere.[60] Briefly, the activated samples were in a vacuum line exposed to 60 mbar ammonia gas (Westfalen, Germany). After 10 min, the excess ammonia was desorbed at 453 K for 2 h. The Si(OH) group density was derived from an integration of the total ^{1}H MAS NMR signal before loading ammonia. It was subsequently corrected for the BAS density derived after ammonia loading. The external standard for ^{1}H MAS NMR quantification was a dehydrated H,Na-Y (35% ammonium exchanged). Loadings with triphenylphosphine (TPP) were performed in a glove box purged with N_2, as described elsewhere.[61] Briefly, approximately 100 mg of dehydrated sample material was mixed with calculated amounts (depending on the total BAS density) of solid TPP (1 to 10 mg) in a glovebox. Then, dichloromethane (DCM) (approx. 1 mL) was added to the mixture and stirred, equilibrated for 1 h, and the sample was finally placed in a desiccator purged with N_2 for a minimum of 2 days to remove the DCM again. The external standard for the ^{31}P MAS NMR measurements was a VPI-5 zeolite in fully hydrated state.[62,63] The measured NMR spectra were evaluated using TopSpin and Dmfit.[64] *In situ* UV/vis spectroscopy was performed using an AvaLight DHS source connected with an Avaspec 2048 spectrometer and the reactor using an HPSUV1000A glass fiber from Oxford Electronics. The optical fiber was placed *ca.* 1 mm above the catalyst in a fixed bed reactor. Prior to starting the flow, reference UV/vis spectra were recorded and subsequently automatically subtracted.

2.3. Catalytic testing

Before catalytic testing, all materials were pressed and sieved to achieve a particle size distribution between 200 and 315 μm. To suppress the effects of the residence time and heat, the catalyst materials were diluted with sea sand (Grüssing, Germany) to a uniform catalyst bed height of 5.3 to 5.6 cm in a fixed bed reactor with an inner diameter of 7 mm. The applied reaction conditions were previously optimized for BTEX formation with $p_{Ethanol}$ = 0.3 bar, T = 673 K, WHSV = 1 or WHSV = 3.[25] The activation of the materials was performed *in situ* in a nitrogen flow of 50 mL min^{-1} by heat treatment at 383 K for 1 h using a heating rate of 3 K min^{-1}. Then, the temperature was increased to 723 K with a heating rate of 1.9 K min^{-1}. After 0.5 h at 723 K, the temperature was reduced to the reaction temperature of 673 K. Ethanol was fed into the reactor by a nitrogen flow of 15 mL min^{-1} that passed a saturator filled with ethanol-containing chromosorb at a constant temperature of 326.5 K. All piping after the saturator until the GC inlet was heated above 393 K to avoid condensation. Ethylene feed was fed directly into the reactor from a mixture of 40.2% ethylene in N_2 (prepared by Westfalen, Germany). The product stream was analyzed using a Hewlett Packard series II 5890 GC, equipped with an FID and an Agilent PoraPLOT Q column (52.5 m, 0.32 mm, 10 μm). GC measurements were performed every 53 minutes. The selectivity was determined starting after 68 min by averaging the data from 7 subsequent measurements at WHSV = 1 h^{-1}. By applying thermogravimetric analysis (TGA) on a Setaram Setsys 16/18, the coke content of the completely deactivated

catalysts was determined. Briefly, the samples (0.1 mg) were heated in synthetic air flow up to 1223 K (holding for 2 h) with a heating rate of 10 K min^{-1}. The total coke content was corrected for the mass of the (inert) sea sand, and refers to the coke on the zeolite mass only.

3. Results and discussion

3.1. Physicochemical characterization of materials

First, the properties of the applied catalysts are discussed. The nomenclature used herein includes the zinc loading in wt%, followed by the material. Z indicates a microporous ZSM-5 and D a desilicated, micro-/mesoporous ZSM-5 as parent of the exchange, which is followed by the Si/Al ratio of the host material. For example, 0.7Zn/Z11 is a microporous parent material (parent Si/Al = 11) with 0.7 wt% zinc, while 2.0ZnD29 is a desilicated material originating from the parent D29 (that was derived from Z29 with a Si/Al of 29 by desilication) and with 2.0 wt% zinc. The physicochemical properties of the materials used herein were investigated before and after modification by zinc and/or desilication by standard techniques. The key properties are summarized in Table 2 and further details on the applied parent materials are found elsewhere.[25] X-ray powder diffraction patterns of all material are depicted in Fig. S1 of the ESI,† and show the typical reflexes of the MFI crystal structure. The crystallinity is largely maintained after desilication or ion exchange. This indicates that the structure of the materials was also maintained after treatments, and neither competing phases nor amorphous deposits were formed. SEM images of two microporous samples and two desilicated samples are shown in Fig. 1. It is found that the materials form small crystallites of comparative dimension and agglomeration, both before and after desilication.[39] N_2-physisorption was applied to probe the porosity and surface of the materials. For the microporous ZSM-5, a surface area of 420 m^2 g^{-1} for the Z11 and of 360 m^2 g^{-1} for the Z29 was verified. Introduction of Zn^{2+} does not lead to systematic changes of the surface area. Upon desilication, the BET surface area and the associated mesopore volume (V_{meso}) increase to up to 438 m^2 g^{-1} for D11 and 435 m^2 g^{-1} for D29, and to 0.30 ml g^{-1} for D11 and 0.33 ml g^{-1} for D29, respectively.[38] In agreement with previous findings, the desilication leads to a significant mass loss of 20 to 30% of the respective zeolites.[38]

The present aluminum species were characterized by ^{27}Al MAS NMR spectroscopy, as desilication can cause formation of undesired extra-framework aluminum deposits that may either block pores or give rise to the formation of Lewis acid sites (LAS).[46,47] The ^{27}Al MAS NMR spectra are shown in Fig. S2 of the ESI,† and all materials have a main signal at ~54 ppm associated with tetrahedral aluminum in framework positions.[25,65,66] A significant broadening of this peak in the presence of Zn (compared also to the spectra of the parents[38]) is not found. As no quadrupolar broadened peak forms, the presence of hydrated ZnO can be excluded.[56] The materials 0.7Zn/Z11, 1.0Zn/Z11, 2.5Zn/Z11, and 3.1Zn/Z11 show weak peaks of pentahedral or distorted, tetrahedral aluminum as broad shoulders at ~35 ppm that vanish upon desilication. Weak peaks of extra framework aluminum at −1 ppm are found in the case of D11. However, these peak intensities decrease after Zn-loading. Materials based on the microporous parent Z29 do not show any peaks at ~0 ppm. Therefore, only negligible amounts of extra framework aluminum are present. This is in line with previous findings that Zn loading does not lead to ZSM-5 dealumination.[56] In terms of Brønsted acid sites (BAS) and LAS, the acidity of the materials was tested by applying NH_3 as probe molecule and subsequent desorption at 453 K, as described elsewhere.[60] The adsorption of ammonia leads to the protonation of the latter, and the intensity of the formed symmetric ammonium peak is thus proportional to the number of accessible BAS. Due to a missing signal intensity in the range up to 4 ppm

Table 2 Data from the physicochemical characterization of the materials under study

Material	Si/Al ratio[a]	Zn/Al ratio	Crystallinity[b] [%]	BAS[c] [mmol g^{-1}]	External BAS[d] [mmol g^{-1}]	(OH)-density[e] [mmol g^{-1}]	BET surface area [m^2 g^{-1}]
Z11	11	—	90	0.66	—	0.31	420
D11	12	—	85	0.74	0.03	0.75	438
0.7Zn/Z11	11	0.09	89	0.77	—	0.84	410
1.0Zn/Z11	10	0.12	84	0.41	—	0.90	399
2.5Zn/Z11	11	0.34	87	0.31	—	0.91	418
3.1Zn/Z11	12	0.44	90	0.32	—	0.63	390
1.5Zn/D11	12	0.20	85	0.69	—	0.75	415
2.0Zn/D11	12	0.27	83	0.45	—	0.88	408
Z29	29	—	95	0.48	—	1.16	360
D29	26	—	90	0.68	0.02	0.48	435
0.5Zn/Z29	28	0.14	92	0.43	—	0.43	421
0.7Zn/Z29	29	0.18	86	0.34	—	0.47	445
0.6Zn/D29	25	0.16	87	0.61	0.01	0.42	431
1.0Zn/D29	26	0.26	87	0.38	—	0.75	413

[a] Determined *via* ICP-OES, error ±1. [b] From X-ray diffraction patterns relative to amorphous scattering. [c] From ^1H MAS NMR after NH_3 adsorption, error ±5%. [d] Determined by ^{31}P MAS NMR after TPP adsorption, error ±0.005 mmol g^{-1}. [e] From ^1H MAS NMR after subtracting BAS density.

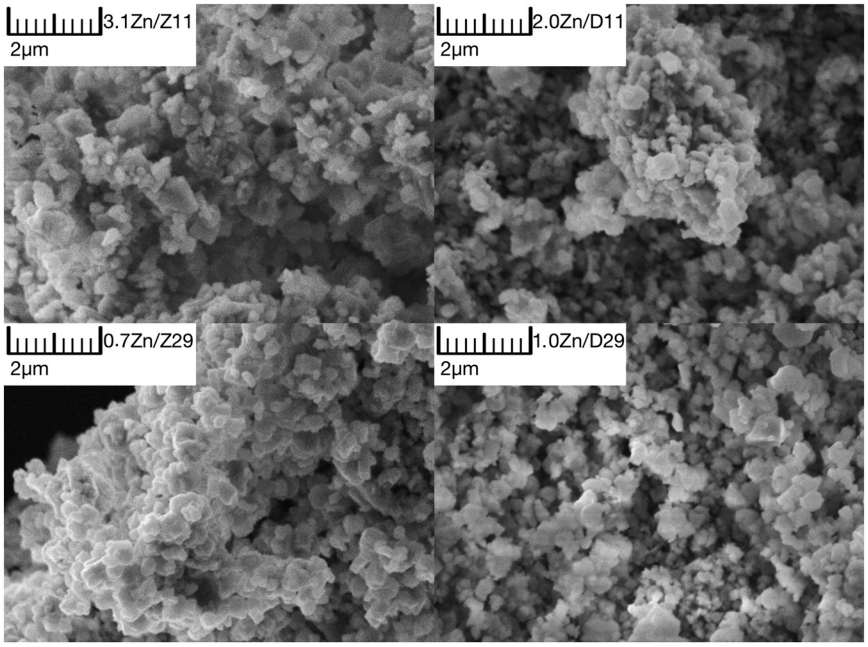

Fig. 1 SEM images of the catalysts 3.1Zn/Z11, 2.0Zn/D11, 0.7Zn/Z29, and 1.0Zn/D29.

after ammonia desorption, we conclude that no strong LAS were detected (<0.01 mmol g^{-1}). Conversely, as shown in Table 2, BAS densities are found, as determined after NH_3-loading by quantitative ^{1}H MAS NMR spectroscopy. It is noteworthy that this value refers to strong LAS that can adsorb the probe ammonia at a similar strength as aluminum- or boron-associated LAS.[67,68] Since each cation can potentially be regarded as LAS, the given number will change with the applied characterization technique. For example, alkali metal cations can be regarded as weak LAS, although they do not interfere with methanol conversion.[69] However, for catalysis, it is important to know whether the LAS is capable of interfering. This would be the case if a strong LAS at zinc acted primarily as LAS, instead of acting as the bifunctional dehydrogenation component. As far as we know, this is not the case herein. In other words, the given numbers do not exclude that weak LAS (for example, at zinc) are found by applying other characterization techniques; it only assures that the strong LAS are absent.

Desilication leads to an increased BAS density, which is a phenomenon known from literature and caused by better access to the micropore system due to the removal of blocked pores.[38,70] A similar increase is observed when the microporous parents were herein ion exchanged with Zn. It is also noted that the Si(OH)-density increases significantly upon desilication, which is in agreement with the literature. Similarly, a slight increase of the total (OH)-density is found upon ion exchange with Zn^{2+}, presumably resulting from the minor formation of the $Zn(OH)^+$ species. According to literature, such species are observed in high loadings with Zn^{2+}, as the amount of paired BAS sites in the zeolite structure (that can compensate a twofold positive charge) is naturally limited.[56] Furthermore, these numbers indicate that the LAS-causing extra-framework aluminum was partially removed, which is in agreement with the ^{27}Al MAS NMR spectra.

The location of the catalytically active BAS is crucial for ensuring a proper shape selectivity in the ethanol conversion. In the case of the microporous parents applied herein, only a negligible external BAS density is detectable (<0.01 mmol g^{-1}).[25] However, as result of the desilication, some BAS could be located on the outer surface or in macro- and mesopores. Thus, the amount of external BAS was determined by applying triphenylphosphine (TPP) as a probe molecule (see Table 2).[61] The respective ^{31}P MAS NMR spectra of the TPP loaded zeolites are shown in Fig. S3 of the ESI,† and the external BAS is indicated by a peak caused by protonated $TPPH^+$ at a shift δ_{31P} = ~6 ppm. Thus, upon desilication, minor amounts of BAS form on the external surface or in the macro- and mesopores. However, the vast majority of BAS remains inside the shape-selective pore system. This is in agreement with previous studies on the desilication and BAS location.[38] Despite the parent D11 showing minor amounts of external BAS, the Zn-exchanged materials 1.5Zn/D11 and 2.0Zn/D11 show no peak at ~6 ppm. Increased amounts of TPP were loaded; however, these did not lead to any peak associated with $TPPH^+$. We conclude that the external BAS are preferentially exchanged with zinc cations. This is reasonable, as external ion exchange sites are very easily reached by Zn^{2+} ions and can also later be complexed easily by TPP, as enough space around these cations is available. It should be noted that especially on desilicated samples, an additional ^{31}P peak at δ_{31P} = ~16 ppm appears after loading TPP in varying intensity, but only if Zn is present. Presumably, this peak is thus caused by formation of a $Zn(TPP)_x$ complex. A similar complexation of other metals (Pt, Pd, Ru, Rh) on the surface with TPP was described previously.[61–63] As TPP cannot

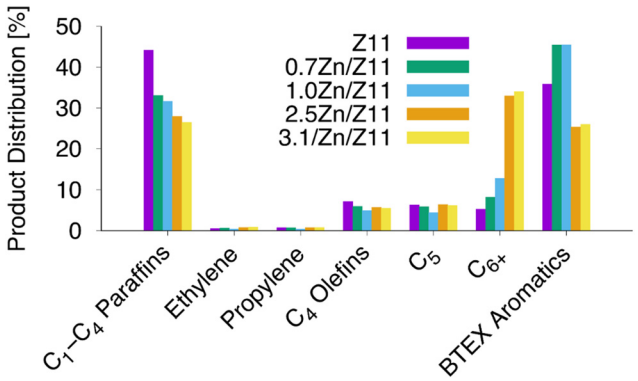

Fig. 2 Effect of zinc on the ETA product distribution over Z11-derived samples at WHSV = 1.0 h^{-1}, T = 673 K, p(ethanol) = 0.3 bar, and flow = 15 mL min^{-1}.

enter micropores, the formed $Zn(TPP)_x$ complexes are located in mesopores or on the external surface.[61] This again supports the preferential exchange of un(*shape*)selective BAS on the external surface. Thus, it is shown that the external sites that form upon desilication are preferentially ion-exchanged with Zn^{2+}, and therefore not detectable as BAS upon loading TPP. This is completely reasonable, as the two-fold charged Zn^{2+} can bind to these external sites without having to pass a micropore. In summary, the applied materials are intact, accessible for potential reactants, and show properties that are expected from literature on similar systems.

3.2. Investigation of the materials in the ethanol-to-aromatics (ETA) conversion

3.2.1. Zn-loading of microporous ZSM-5. BAS are the catalytically active sites in the ETA conversion. In order to synthesize improved bifunctional catalysts, it is common practice to apply the exchange with transition-metals. For determining the effect of Zn, microporous Z11 materials with Si/Al = 11 were first exchanged and investigated in the ETA conversion (see Fig. 2). Original data from the catalytic testing are found in Fig. S4–S15 in the ESI.† The tabulated product distributions are found in Table S2 in the ESI.† Table 3 provides performance descriptors of the reaction. A schematic overview over the reactions that lead to the formation of aromatics is found elsewhere.[12,21] Regarding the effect of water in the feed, either as part of the C_2-unit or as a co-reactant, it is recommended to refer to previous work.[25] Briefly, small amounts of water up to a $C_2:H_2O$ stoichiometry of 1 : 0.5 benefit the formation of aromatics, but larger amounts hinder it. Furthermore, an ethylene-pure feed increases lifetime and total aromatic production more than a diethylether feed, while an ethanol feed gives the poorest results.

Compared with the parent Z11, a vastly decreased amount of C_1–C_4 paraffins is found for the Zn-loaded samples. Conversely, the contribution of the C_{6+} fraction increases with increased Zn-loading. The content of BTEX aromatics has an optimum at a Zn-loading between 0.7 and 1 wt%. With lower or higher zinc loadings, the amount of BTEX aromatics thus decreases, which is in line with a balance between the two catalytically active sites in the bifunctional system. An increase in BTEX aromatics formation upon Zn-loading thus agrees with the literature on Zn,H-ZSM-5 catalysts.[59] If the Zn-loading is increased, a large C_{6+} fraction forms. However, fewer aromatization reactions occur, which is the reason for the decreased BTEX content that we observe. We also remark that the amounts of aromatics and paraffins are not stoichiometric anymore, as expected when dehydrogenation (instead of hydrogen transfer) is dominant due to Zn-incorporation. This effect was described previously.[50,52]

Table 3 Data on lifetime/deactivation, coke, conversion capacity (CC) of C_2-units (usually ethanol) and the total amount of aromatics (TA) formed until deactivation ($X_{ethylene}$ < 20%) at WHSV = 3.0 h^{-1}, T = 673 K, p(ethanol) = 0.3 bar, and flow = 15 mL min^{-1}

Material	Lifetime[a] [h]	Coke[b] [%]	CC C_2 [g g^{-1}]	TA BTEX [g g^{-1}]	TA BTEX/CC C_2
Z11	18.1	12.1	35.2	8.8	0.25
0.7Zn/Z11	24.5	5.4	53.9	10.1	0.19
1.0Zn/Z11	20.1	6.5	41.6	9.2	0.22
2.5Zn/Z11	14.2	10.4	28.9	3.4	0.12
3.1Zn/Z11	12.9	10.5	28.2	4.1	0.15
D11	25.1	10.2	57.5	10.6	0.18
1.5Zn/D11	13.4	8.9	28.6	6.8	0.24
1.5Zn/D11[c]	32.3[c]	13.1[c]	63.8	15.9	0.25
2.0Zn/D11	8.2	10.2	17.8	4.8	0.27
Z29	31.8	7.0	64.8	10.9	0.17
Z29[c]	95.2	10.0	124.1	22.6	0.18
0.5Zn/Z29	29.9	10.8	51.1	4.9	0.10
0.5Zn/Z29[c]	105.0	7.7	173.1	22.0	0.13
0.7Zn/Z29	20.4	6.6	30.7	3.1	0.10
D29	75.6	9.2	154.2	16.9	0.11
0.6Zn/D29	42.9	5.8	73.0	7.9	0.11
0.6Zn/D29[c]	118.8[c]	5.5[c]	206.0	31.6	0.15
1.0Zn/D29	30.3	6.7	42.6	4.9	0.12

[a] From catalytic testing; >80% ethylene yield. [b] From TGA. [c] Ethylene feed under similar conditions.[25]

Apart from selectivity, the lifetime is a critical parameter in the ETA conversion. A low Zn-loading causes longer lifetimes of the catalysts 0.7Zn/Z11 and 1.0Zn/Z11 (24.5 and 20.1 h, respectively) compared to the parent Z11 (lifetime 18.1 h), as shown in Table 3. This is, again, in line with literature expectations that compare Zn-exchanged ZSM-5 with Zn-free parents.[59] However, higher Zn-loadings lead to decreased lifetimes, similar to what was previously observed in the MTO conversion.[50] A potential explanation for the initially increased lifetime is the reduced amount of BAS present, which extends the ETA lifetime.[25] To account for a different framework Si/Al with respect to BAS-density, the influence of Zn-loadings was investigated for a second ZSM-5 family based on the parent Z29, as shown in Fig. S18 in the ESI.† A similar picture is observed. Again, the C_1–C_4 paraffin fraction decreases, while the BTEX aromatic and the non-aromatic C_{6+} fractions increase. This results in a reduced BTEX content after Zn-loading. However, for the Z29 family also the lifetimes decrease. This demonstrates that the effect of prolonged lifetimes for the Z11-derived catalysts originated from a changed BAS density. It was not caused by the reactivity of the Zn^{2+}-cations. Conclusively, an intermediate Zn-loading benefits an increase in the BTEX production in the steady state on ZSM-5 catalysts with different Si/Al ratio with respect to BAS density. Zn-loading also reduces the amount of coke formed on the Z11 family, whereas for the Z29 family only higher Zn-loadings (0.7Zn/Z29) reduce the finally observed coke content.

If total conversion capacities (CC) or total BTEX aromatic production (TA) over the whole lifetime are taken into account (see Table 3), the picture becomes complicated due to the dynamic change in the product distribution over time-on-stream (TOS), as observed in the original data in Fig. S4 to S17 in the ESI.† Over time, the share of BTEX aromatics decreases as result of the coking and changed residence time. This is in line with previous studies on ETA conversion.[25,38,39] For the Z11-family, low Zn-loadings lead to high conversion capacity and high total formation of BTEX over the complete TOS, while increasing the loadings over an optimum leads to decreased values again. This is a result of faster coking due to the increased production of aromatics. For the Z29-family, the parent outperforms its Zn-loaded children in both conversion capacity and total BTEX production. Hereby, an optimized BAS density overcompensates the effect of Zn-loading. Thus, answering the question if a Zn-loading is beneficial for increasing the BTEX production depends on the Si/Al ratio of the parent, but also significantly on how long the ETA conversion runs. Nevertheless, it is most important to note two things: (1) that Zn-loading reduces the amount of cheap paraffins, and (2) that Zn-loading increases the formation of olefins and aromatics that have a higher value for synthetic chemistry and fuels. In particular, these positive selectivity changes affect the product distribution in the first third of the total TOS.

3.2.2. Combination of Zn-loading and desilication. Within this section, desilicated catalysts with and without Zn-loading are compared to their respective microporous parents Z11 and Z29, respectively (see Fig. 3 and 4). If only desilication is applied to the Z11 parent, a procedure that leads to the hierarchical D11, we observe marginal changes in the product distribution (see Fig. 3). However, the lifetime of the catalyst D11 increases from 18 to about 25 h time-on-stream (TOS) due to the introduced mesoporosity. This is the reason for an increased D11 conversion capacity of 57.5 g g^{-1} (parent: 35.2 g g^{-1}) for ethanol. All observations are in line with literature on desilicated ZSM-5 applied in the ETA conversion.[38,43] As for Zn-loaded microporous materials, the contributions of the C_{6+} fraction increases, while the C_1–C_4 paraffins decrease tremendously (see Fig. 3). In parallel, the lifetime until deactivation, conversion capacity, and the total amount of BTEX produced decrease (see Table 3). A decreased lifetime upon Zn-loading of ZSM-5 is well-known from application of Zn–ZSM-5 catalysts in the MTO conversion, and is caused by the increased production of aromatics as coke-precursors.[50] The composition of the BTEX-fraction changes with the BAS density, in agreement with the literature.[25] A combination of increased BTEX production, but decreased lifetime, results in decreased total yields for our samples (see Table 3). Again, the total values are calculated until full deactivation, and thus show an average of the strongly decreasing BTEX amount in the product stream during the deactivation period. Thus, a short steady state is followed by a steadily decreased BTEX content, as observed for ~2/3 of the total lifetime of the investigated catalysts (see Fig. S4–S15 in the ESI†). Next, the combination of desilication and Zn-loading is discussed at a significantly higher Si/Al ratio for the Z29-family (see Fig. 4). Again, the product distribution is widely maintained after desilication. A slightly increased paraffin content is the result of the ~40% increased BAS density of D29 compared to Z29.[38] A more than doubled lifetime is observed for D29 compared to the parent Z29. Thus, the desilication is obviously more effective on the parent Z29 than on the parent Z11. Upon Zn-loading of D29, as observed previously for Zn-loadings on D11, the amount of BTEX

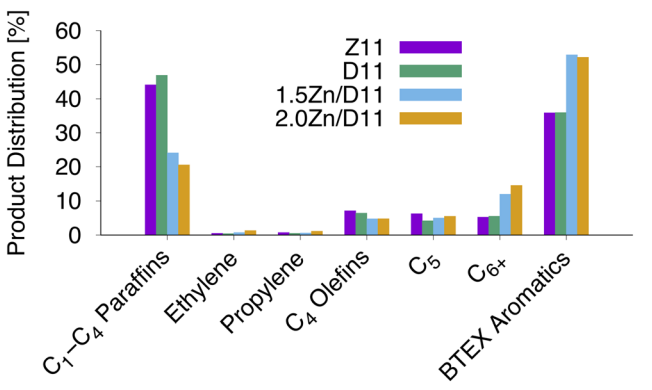

Fig. 3 Effect of zinc and desilication on ETA product distribution over D11-derived samples at WHSV = 1.0 h^{-1}, T = 673 K, p(ethanol) = 0.3 bar, and flow = 15 mL min^{-1}.

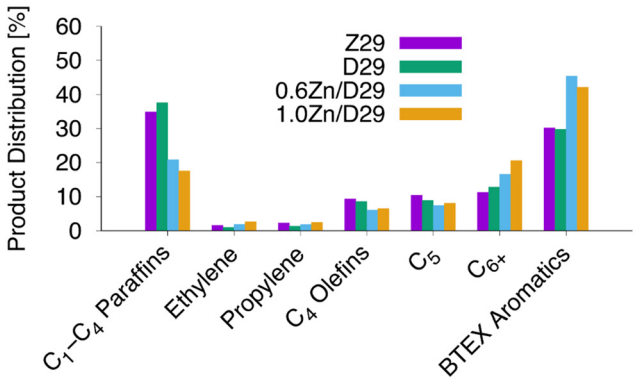

Fig. 4 Effect of zinc and desilication on ETA product distribution over D29-derived samples at WHSV = 1.0 h^{-1}, T = 673 K, p(ethanol) = 0.3 bar, and flow = 15 mL min^{-1}.

aromatics and the C_{6+} fraction increases, while the amount of C_1–C_4 paraffins decreases. Again (as in the case of the Z11-family), the lifetimes decrease significantly upon Zn-loading. This leads to decreased total conversion capacities and total BTEX yields. Fig. 5 also conveys changes of the product distribution over TOS.

Of particular interest is the composition of the BTEX fraction (see Table 4). All investigated product streams contain benzene (C_6) as the minor component with up to 10.1% of the total BTEX content. The BTEX products are rich in toluene (C_7) and the C_8-fraction with ethylbenzene, *o*-, *m*-, and *p*-xylene (which we could not completely separate). However, it can be stated that *o*-xylene is only present in small amounts, while ethylbenzene and/or *p*-xylene account for the main share of the C_8-fraction. Throughout the investigated catalysts, we find surprisingly similar compositions of the BTEX fraction. The found distribution of the BTEX fraction is in line with previous findings.[25] In particular, microporous and desilicated catalysts show roughly comparable compositions. Minor changes in BTEX composition can be caused by a change in the BAS density, as previously reported.[25] Zn-containing samples show a lower C_6 content and usually a larger C_8-fraction than the respective parents. The highest amount of C_8-fraction products originates from catalysts with a combination of desilication and Zn-exchange. For 0.6Zn/D29 and 1.0Zn/D29, up to 70% of the BTEX content forms a C_8-fraction. Meanwhile, in parallel, only <3% benzene (C_6) and <30% toluene (C_7) are produced. Thus, changes in the BTEX composition are observed if the catalysts are desilicated and/or exchanged with Zn^{2+}-cations. Again, it

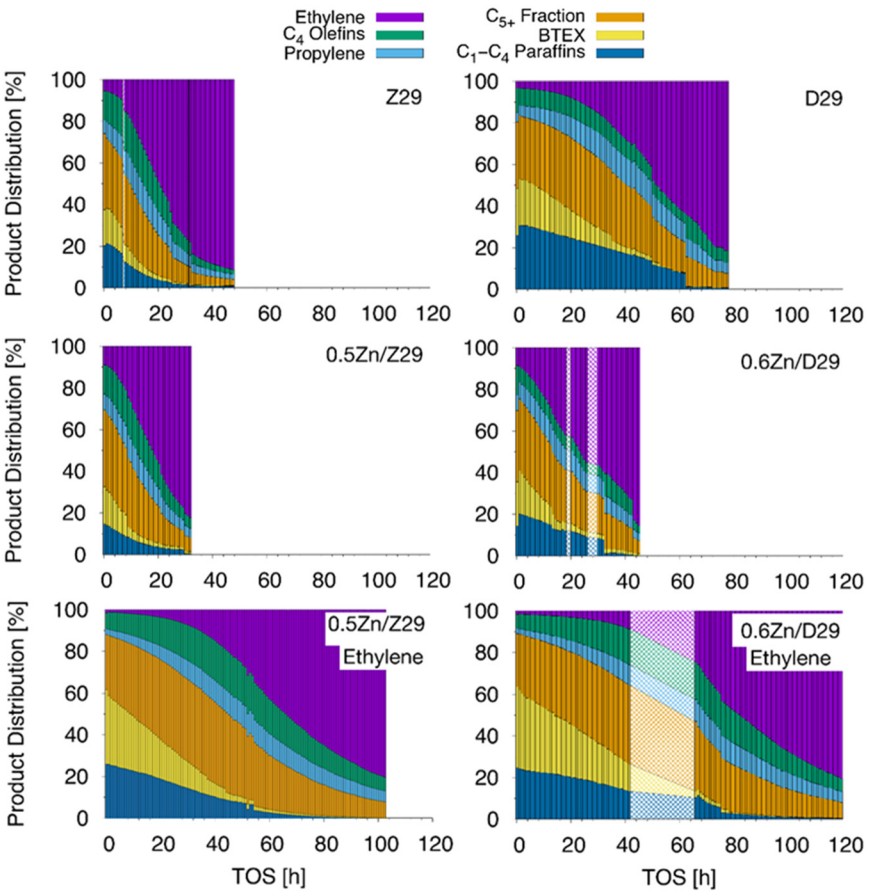

Fig. 5 Effect of zinc and desilication of Z29-derived samples on ETA conversion at WHSV = 3.0 h^{-1}, T = 673 K, p(ethanol) = 0.3 bar, and flow = 15 mL min^{-1} (top, middle) or with comparable ethylene feed (bottom). Missing GC-measurements are indicated by lighter color approximations to guide the eye.

Table 4 The amount of BTEX aromatics in product distribution is given at TOS = 120 min. This 100% BTEX content is then broken down into shares of C_6-, C_7-, and C_8-range aromatics. Data taken at WHSV = 3.0 h^{-1}, T = 673 K, p(ethanol) = 0.3 bar, and flow = 15 mL min^{-1}

Material	BTEX[a] [%]	C_6 [%]	C_7 [%]	C_8 [%]
Z11	27	6.3	39.3	54.4
0.7Zn/Z11	35	0.5	38.8	60.7
1.0Zn/Z11	38	4.1	36.3	59.5
2.5Zn/Z11	21	4.8	33.1	62.1
3.1Zn/Z11	23	3.3	30.1	66.6
D11	31	10.1	44.3	45.6
1.5Zn/D11	37	2.8	31.5	65.7
1.5Zn/D11[b]	48	6.1	35.2	58.8
2.0Zn/D11	34	2.4	29.1	68.5
Z29	17	7.5	32.9	59.6
Z29[b]	29	6.7	40.8	52.5
0.5Zn/Z29	16	2.6	31.9	65.5
0.5Zn/Z29[b]	31	5.0	38.9	56.1
0.7Zn/Z29	13	2.5	29.2	68.2
D29	22	5.9	37.7	56.4
0.6Zn/D29	19	2.3	27.5	70.2
0.6Zn/D29[b]	37	5.5	39.4	55.1
1.0Zn/D29	16	2.3	28.7	68.9

[a] Total BTEX content of product distribution at TOS = 120 min. [b] Ethylene feed under similar conditions.[25]

depends on the needed products and the availability of product streams that consume the by-products to identify the most competitive catalyst for the conversion of ethanol. Thus, the following discussion on the "best" catalyst will focus on the BTEX content in general.

For all investigated catalyst systems, the BTEX contents are initially high. However, they drop significantly after about 1/4 of the total lifetime. The BTEX content is higher for desilicated catalysts with and without Zn. In other words, the drop in BTEX content then occurs later, after 1/3 of the total lifetime and at much higher BTEX levels. The strong changes in product distribution during the course of the reaction become clear if one compares the high share of BTEX in the averaged product distribution of runs 2 to 8 in Table S2† with the ratio between the total BTEX production and total conversion capacity (TA BTEX/CC C_2) in Table 3. We chose a TOS of 120 min as representative for indicating how efficiently a catalyst can produce BTEX-range products. Overall, the ETA conversion is far shorter in a steady state (regarding BTEX production) than, for example, the MTO conversion.[34] This shorter steady state of the ETA conversion results from the fast formation of aromatics that tend to clog the micropores. The usually lower reaction temperature decreases the cracking activity, and larger non-aromatic hydrocarbons are thus produced. Aromatization of long olefins is one of the last reaction steps that occurs in the reaction chain. No wonder that during the course of the deactivation of ETA catalysts, there are far more long-chain olefins found that have not yet been aromatized, particularly when compared with the MTO conversion.[34] However, these long-chain olefins might likewise be highly interesting and useful for other product streams, which makes the ETA conversion a classical candidate for large-scale operations that are comparable to today's refineries and MTO plants. Conclusively, in an industrial ETA application, the catalysts will presumably be regenerated far before they are fully deactivated. Following the above-made statements, the optimum catalyst must be picked based on the process and used (by-)products. We thus make three suggestions for the "best suited of the catalysts mentioned herein":

(Case 1) A low Si/Al ratio on its own increases the amount of aromatics at the cost of the lifetime.[25] Desilication enhances the lifetime without significantly changing the product composition.[38] Thus, if metal-free catalysts are desired that run until deactivated, desilicated catalysts as D29 alone could be a good option, based on their high TA BTEX (see Table 3). In addition, the parents Z11 and Z29 show a high BTEX formation (however, faster coking).

(Case 2) Most applicants of the catalysts will likely be interested in the question: how much of the converted ethanol is transferred into aromatics? In other words, the highest BTEX production (TA BTEX) per conversion capacity (CC C_2) is desired (see Table 3). This ratio is thus a good criterion to pick a suitable catalyst, if only aromatics are requested and the catalysts run until deactivation. Then, the samples 1.5Zn/D11, 2.0Zn/D11, and the parent Z11 are the best catalysts (TA BTEX/CC C_2 around 0.25).

(Case 3) If the short-chain olefins can be used in other product streams, a zinc-containing sample that minimizes alkane production and a long conversion capacity (CC C_2), *i.e.*, lifetime, is desired. Such a combination requires higher Si/Al ratio, desilication and zinc-exchange. The best combination of the three properties is in particular found for sample 0.6Zn/D29. However, in the end, the optimization of the feed is often more impactful than the catalyst design. The influence of the feed will thus be discussed in more detail in the next chapter.

3.2.3. Feed optimization and UV/vis spectroscopy. An oxygen-free feed optimization can lead to significantly increased aromatic contents and lifetimes, as previously observed for microporous ZSM-5 catalysts.[25] In particular, we applied a pure ethylene feed in an equivalent molar hourly space velocity (MHSV) as the ethanol feed (WHSV = 3 h^{-1}). The original data are found in Fig. S19 to S21 in the ESI,† while key results are tabulated in Tables 3 and 4. It is observed that for the two catalysts 1.5Zn/D11 and 0.6Zn/D29 an ethylene feed outperforms the ethanol feed. For 1.5Zn/D11, changing the feed results in an increased lifetime of 32.3 h compared with 13.4 h for the ethanol feed, accompanied by a slight increase in the total coke content from 8.9% to 13.1%. Both total ethanol conversion capacity and the total BTEX yield are more than doubled from 28.6 to 63.8 g g^{-1} and from 6.8 to 15.9 g g^{-1}, respectively. These are the highest values reported so far for the Z11-family. They result from the higher lifetime when applying the ethylene feed, and an associated steadier BTEX production. It is noteworthy that during the first ~10 h TOS, BTEX contents close to 50% are found, which is the highest reported within this study.

However, BTEX are well-known coke precursors; thus, the overall short lifetimes of the Z11-family are reasonable. Hence, for the Z29-family a longer lifetime comes at the cost of the BTEX content in the product distribution. The composition of the BTEX content changes with the feed (see Table 4). Ethylene feed increases the share of benzene (C_6) and toluene (C_7) in the BTEX fraction, at the cost of the C_8-fraction for all compared samples. For 0.6Zn/D29, changing the feed resulted in a nearly tripled lifetime of 118.8 h, compared with 42.9 h for an ethanol feed. Comparison of 0.6Zn/D29 with the very similar but not desilicated 0.5Zn/Z29 indicates that desilication upon ethylene feed not only leads to a longer lifetime (118.8 *vs.* 105.0 h), but also to a significantly higher production of total BTEX contents (31.6 *vs.* 22.0 g g^{-1}). The longer lifetime of 0.6Zn/D29 is accompanied by a slightly lower coke content of 5.5% compared to 5.8%. As the lifetime significantly increases, the total ethanol conversion capacity more than doubles from 73.0 to 206.0 g g^{-1} and the total BTEX yield quadruples from 7.9 to 31.6 g g^{-1}, respectively. The latter is the highest total BTEX yield in this study. Thus, in terms of total BTEX yield, 0.6Zn/D29 outperforms its desilicated precursor, D29, the catalyst 1.5Zn/D11, and the parent Z29 with the ethylene-feed (lifetime: 95.2 h, conversion capacity 124.1 g g^{-1}, total BTEX yield 22.6 g g^{-1}, see (ref. 25)) all by a factor of about 2.

To further elucidate the effect of the ethylene feed on our samples, we conducted *in situ* UV/Vis spectroscopy. This *in situ* spectroscopy is reportedly complicated by a coke-free initiation zone for ethanol dehydration.[21] We were nevertheless successful in investigating the coke formation. The initial 50 min of the reaction for the chosen catalysts are plotted in Fig. 6. We compare the microporous parent Z29 with its Zn-loaded (0.5Zn/Z29) and Zn-loaded and desilicated (0.6Zn/D29) counterparts, and all three with ethanol and ethylene feed, respectively. It is found that the intensity of the absorbance bands in the UV/vis region between 200 and 600 nm increases rapidly for the parent Z29 and in particular for the Zn-loaded sample 0.5Zn/Z29 upon feeding ethanol. Considerably slower is the coking of the desilicated sample 0.6Zn/D29. This is in agreement with the above-discussed findings on the enhancement of lifetime by desilication, and agrees with previous studies.[38] For each of the three samples, the band intensity increases are slower when, instead of ethanol, an ethylene feed was applied. This is also indicated by the zero absorbance throughout the first measured spectra for all three samples. The order of the

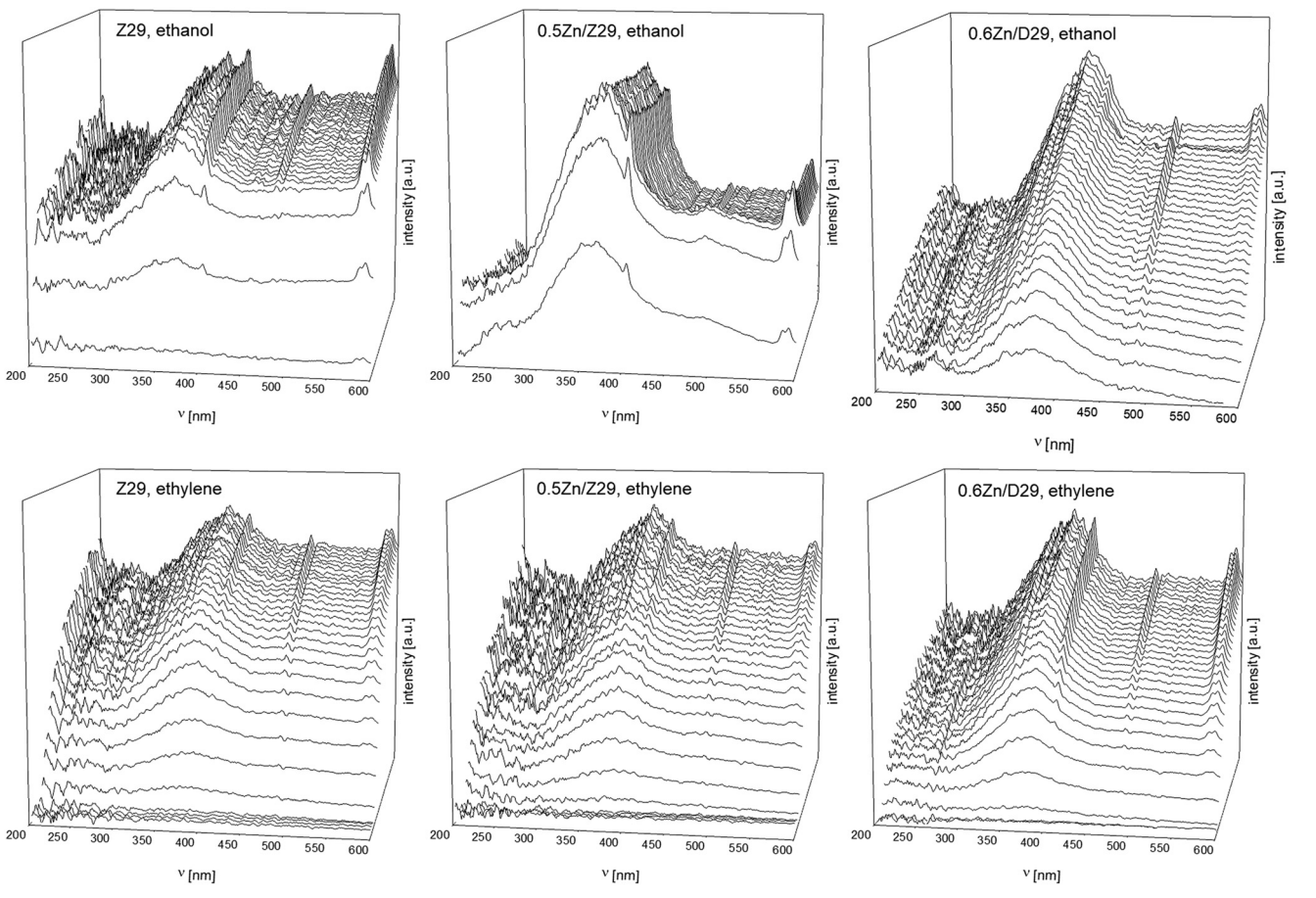

Fig. 6 *In situ* UV/vis spectra on the coking behavior of samples during the first 50 min of reactant flow, namely, Z29 (left), 0.5Zn/Z29 (middle), and 0.6Zn/D29 (right) with ethanol (top) and ethylene (bottom) feed at T = 673 K, p(ethanol) = 0.3 bar, and flow = 15 mL min^{-1}.

coking speed, directly followed by UV/vis spectroscopy, resembles the total lifetimes in catalytic testing of the respective catalysts. These were 29.9 h (Z29), 31.8 h (0.5Zn/Z29), and 42.9 h (0.6Zn/D29) for an ethanol feed; and 95.2 h (Z29), 105 h (0.5Zn/Z29), and 118.8 h (0.6Zn/D29) for an ethylene feed. Thus, the *in situ* UV/vis measurements support a faster coke built-up if ethanol feed is used instead of ethylene feed.

Next, the identity of the found coke species in Fig. 6 shall be addressed. Up to 240 nm bands due to dienes are found,[71] followed by those of the uncharged monocyclic, polyalkyl-aromatics at 254–280 nm.[71,72] From *ca.* 275 to *ca.* 410 nm, bands for charged, alkylated cyclohexene- or monocyclic aromatics appear,[72–74] like hexamathylbenzenium at *ca.* 390 nm.[75] Subsequently, bands of polycyclic aromatics, like naphthalene, occur up to *ca.* 470 nm.[34,72,76] It is noted that the maximum absorbance for the microporous samples with ethanol feed (Z29 and 0.5Zn/Z29) is found at a lower nm-range below 400 nm. These bands result from a superposition of the coke-precursor and coke species, as presumably carbenium ions remain trapped within the pores of the samples. In contrast, after a desilication of the sample, the UV/vis spectra of 0.6Zn/D29 show a slower increase in intensity. In particular, a far lower intensity below 350 nm is observed then for 0.5Zn/Z29. The maximum UV/vis absorbance of the samples during application of an ethylene feed is located at higher nm-values. This indicates that the remaining species are to a higher extent composed of polyaromatic coke. The UV/vis spectra show negligible absorbance below 300 nm. Bands here would correspond to trapped, uncharged olefins or aromatics. However, these short-chain species are absent when conducting the ETA conversion. Notably, they are observed if olefin-cracking pathways during MTO conversion are dominant.[34] In contrast, a fast buildup of alkylated aromatics is observed in the case of ethanol feed, especially for 0.5Zn/Z29. These aromatics remain trapped inside the pores. The fast pore clogging is reflected by a shorter lifetime and in line with the shown catalytic testing. Chowdhury *et al.*[12] observed the formation of oxygenates, propionate and acetate, when applying ethanol feed. It is noteworthy that such oxygenates lead to a fast coke formation in the MTO conversion.[77] In-line with the hypothesis that absence of oxygenates is crucial for enhancing also the ETA lifetimes, the coke formation for the ethylene feed is slower. The spectra are reminiscent of the *in situ* UV/vis spectra reported for MTO catalysts with low BAS density and high propylene production.[34] In parallel to these spectra, a high production of BTEX aromatics during catalytic testing further supports that the formed aromatics leave the pores more easily in the case of an ethylene feed. It is thus reasonable that an ethylene feed avoids the formation of highly reactive oxygenates that induce a very fast pore blocking and trapping of aromatics inside the catalyst pores.[25] Thus, combined catalytic testing and *in situ* UV/vis spectroscopy confirm a slower coke formation if ethylene is used as feed instead of ethanol.

4. Conclusion

A combination of desilication, ion exchange with zinc, and suitable reaction parameters increases the production of BTEX aromatics from ethanol. Desilication enhances the lifetime in the ETA conversion by introducing mesopores, without significantly affecting the product distribution. In BAS-rich ZSM-5 catalysts, the BTEX aromatics and aliphatics are produced in a stoichiometric ratio. An ion exchange with Zn^{2+}-cations decouples aromatic and aliphatic production. The zinc opens a dehydrogenation pathway that leads to decreased amounts of undesired paraffins. However, the increased production of aromatics also results in faster coking and shortened lifetimes. The ideal Zn-loading of a sample depends on the Si/Al ratio. Beyond an optimum value, too high Zn-loadings will lead to faster deactivation. To increase the lifetime, a desilication was combined with Zn^{2+} exchange. The loading with TPP revealed that Zn-cations completely exchange the external BAS, and no external acidity persists the ion exchange with zinc. The lifetimes of the catalysts increase if desilicated parents are applied for ion exchange. In such samples, the BTEX content contains up to 70% products from the C_8-fraction and below 30% toluene. The composition of the BTEX content is roughly comparable for all samples. It is usually poor in benzene (<10%), while C_7 and C_8-range products make up the majority of the BTEX fraction. However, the total BTEX yield measured over the full lifetime is significantly influenced by the TOS with respect to deactivation of the catalyst, which might lead to a wrong impression on the performance of the catalyst system. It is thus suggested that the respective catalysts are only utilized until deactivation begins (1/3 of total lifetime) or, alternatively, the formed olefin by-products are likewise used and funnelled into suitable product streams.

A feed change to ethylene further enhances the production of BTEX aromatics and lifetimes, especially for desilicated and Zn-exchanged samples. *In situ* UV/vis spectroscopy confirms a slower built-up of coke species if desilicated samples or an oxygenate-free ethylene feed is applied. The coke built-up is thereby reverse proportional to the found lifetimes of the catalysts. In particular, the Zn-exchange of microporous materials enhances the coking speed to an extent where products become trapped inside the micropores. Desilicated and Zn-exchanged desilicated samples coke significantly slower. The ratio between total BTEX formation per conversion capacity (TA BTEX/CC C_2) is a suggested measure of the share of ethanol that is transferred into aromatics in total. Both TA BTEX and CC C_2 are summarized until the conversion to hydrocarbons, excluding ethylene, drops below 20%. Samples 1.5Zn/D11, 2.0Zn/D11, and the parent Z11 show the highest share of aromatics. Thus an ethylene feed enhances the lifetime, improves the initial BTEX content, and increases the total BTEX amount generated until deactivation, presumably due to the absence of formed oxygenates.

In summary, a combination of desilication, Zn-loading, and feed optimization improves the BTEX production, both in terms of selectivity in the steady state and in the total BTEX yield that is formed. Compared with the microporous parents, the improved catalysts show 50% higher BTEX content, up to 4-fold increased lifetime, and up to 3-fold increased total BTEX yields. These results enable higher efficiency in the ETA conversion, and pave the way to valuable bio-based olefins and aromatics. It is the first proof of a successful combination of these modifications in the conversion of ethanol to aromatics and other hydrocarbons.

Data availability

The data supporting this article have been included as part of the ESI.†

Conflicts of interest

There are no conflicts of interest to declare.

Acknowledgements

The authors thank Heike Fingerle for ICP-OES measurements, Maximilian Schmidt for SEM measurements, and Ann-Katrin Beurer, Dorothea Häussermann, Faeze Tari, Nagme Ay, and Michael Benz for N_2-Physisorption measurements. This work was funded by the Deutsche Forschungsgemeinschaft (DFG, German Research Foundation) under Project 471005971.

References

1 E. T. C. Vogt, G. T. Whiting, A. D. Chowdhury and B. M. Weckhuysen, in *Advances in Catalysis*, ed. F. C. Jentoft, Academic Press, 2015, vol. 58, pp. 143–314.
2 J. Weitkamp, *Solid State Ionics*, 2000, **131**, 175–188.
3 T. F. Degnan, *J. Catal.*, 2003, **216**, 32–46.
4 J. J. Bozell and G. R. Petersen, *Green Chem.*, 2010, **12**, 539–554.
5 N. M. Eagan, M. D. Kumbhalkar, J. S. Buchanan, J. A. Dumesic and G. W. Huber, *Nat. Rev. Chem.*, 2019, **3**, 223–249.
6 E. G. Derouane, J. B. Nagy, P. Dejaifve, J. H. C. van Hooff, B. P. Spekman, J. C. Védrine and C. Naccache, *J. Catal.*, 1978, **53**, 40–55.
7 W. Wang, A. Buchholz, M. Seiler and M. Hunger, *J. Am. Chem. Soc.*, 2003, **125**, 15260–15267.
8 W. Wang and M. Hunger, *Acc. Chem. Res.*, 2008, **41**, 895–904.
9 D. Dittmann, J. Schröder, E. Kaya, J. Mosrati, A. M. Abdel-Mageed and M. Dyballa, *J. Phys. Chem. C*, 2023, **127**, 18962–18970.
10 W. Wang, J. Jiao, Y. Jiang, S. S. Ray and M. Hunger, *ChemPhysChem*, 2005, **6**, 1467–1469.
11 J. N. Kondo, K. Ito, E. Yoda, F. Wakabayashi and K. Domen, *J. Phys. Chem. B*, 2005, **109**, 10969–10972.
12 A. D. Chowdhury, A. Lucini Paioni, G. T. Whiting, D. Fu, M. Baldus and B. M. Weckhuysen, *Angew. Chem., Int. Ed.*, 2019, **58**, 3908–3912.
13 X. Zhou, C. Wang, Y. Chu, J. Xu, Q. Wang, G. Qi, X. Zhao, N. Feng and F. Deng, *Nat. Commun.*, 2019, **10**, 1961.
14 K. Gołąbek, E. Tabor, V. Pashkova, J. Dedecek, K. Tarach and K. Góra-Marek, *Commun. Chem.*, 2020, **3**, 25.
15 H. Knözinger, *Angew. Chem., Int. Ed. Engl.*, 1968, **7**, 791–805.
16 H. Knözinger and R. Köhne, *J. Catal.*, 1966, **5**, 264–270.
17 C.-Y. Wu and H.-S. Wu, *ACS Omega*, 2017, **2**, 4287–4296.
18 R. Himmelmann, E. Klemm and M. Dyballa, *Catal. Sci. Technol.*, 2021, **11**, 3098–3108.
19 J. F. DeWilde, H. Chiang, D. A. Hickman, C. R. Ho and A. Bhan, *ACS Catal.*, 2013, **3**, 798–807.
20 A. Takahashi, W. Xia, Q. Wu, T. Furukawa, I. Nakamura, H. Shimada and T. Fujitani, *Appl. Catal., A*, 2013, **467**, 380–385.
21 K. Van der Borght, R. Batchu, V. V. Galvita, K. Alexopoulos, M.-F. Reyniers, J. W. Thybaut and G. B. Marin, *Angew. Chem., Int. Ed.*, 2016, **55**, 12817–12821.
22 J. C. Oudejans, P. F. Van Den Oosterkamp and H. Van Bekkum, *Appl. Catal.*, 1982, **3**, 109–115.
23 J. Schulz and F. Bandermann, *Chem. Eng. Technol.*, 1994, **17**, 179–186.
24 A. G. Gayubo, A. Alonso, B. Valle, A. T. Aguayo, M. Olazar and J. Bilbao, *Fuel*, 2010, **89**, 3365–3372.
25 D. Dittmann, C. Rieg, Z. Li, E. Kaya and M. Dyballa, *Energy Fuels*, 2023, **37**, 4566–4579.
26 Z. Li, D. Dittmann, C. Rieg, M. Benz and M. Dyballa, *Catal. Sci. Technol.*, 2022, **12**, 5189–5202.
27 Z. Li, C. Rieg, A.-K. Beurer, M. Benz, J. Bender, C. Schneck, Y. Traa, M. Dyballa and M. Hunger, *Adsorption*, 2020, **27**, 49–68.
28 A. J. Marchi and G. F. Froment, *Appl. Catal.*, 1991, **71**, 139–152.
29 A. G. Gayubo, A. T. Aguayo, A. E. Sánchez del Campo, A. M. Tarrío and J. Bilbao, *Ind. Eng. Chem. Res.*, 2000, **39**, 292–300.
30 J. S. Martinez-Espin, M. Mortén, T. V. W. Janssens, S. Svelle, P. Beato and U. Olsbye, *Catal. Sci. Technol.*, 2017, **7**, 2700–2716.
31 Y. Liu, F. M. Kirchberger, S. Müller, M. Eder, M. Tonigold, M. Sanchez-Sanchez and J. A. Lercher, *Nat. Commun.*, 2019, **10**, 1462.
32 S. Müller, Y. Liu, F. M. Kirchberger, M. Tonigold, M. Sanchez-Sanchez and J. A. Lercher, *J. Am. Chem. Soc.*, 2016, **138**, 15994–16003.
33 W. J. H. Dehertog and G. F. Froment, *Appl. Catal.*, 1991, **71**, 153–165.
34 M. Dyballa, P. Becker, D. Trefz, E. Klemm, A. Fischer, H. Jakob and M. Hunger, *Appl. Catal., A*, 2016, **510**, 233–243.
35 M. Mortén, Ł. Mentel, A. Lazzarini, I. A. Pankin, C. Lamberti, S. Bordiga, V. Crocellà, S. Svelle, K. P. Lillerud and U. Olsbye, *ChemPhysChem*, 2018, **19**, 484–495.
36 I. Yarulina, A. D. Chowdhury, F. Meirer, B. M. Weckhuysen and J. Gascon, *Nat. Catal.*, 2018, **1**, 398–411.
37 C. D. Chang, C. T. W. Chu and R. F. Socha, *J. Catal.*, 1984, **86**, 289–296.
38 D. Dittmann, E. Kaya and M. Dyballa, *ChemCatChem*, 2023, **15**, e202300716.
39 D. Dittmann, E. Kaya, D. Strassheim and M. Dyballa, *Molecules*, 2023, **28**, 8046.

40 N. Viswanadham, S. K. Saxena, J. Kumar, P. Sreenivasulu and D. Nandan, *Fuel*, 2012, **95**, 298–304.
41 W. Schwieger, A. G. Machoke, T. Weissenberger, A. Inayat, T. Selvam, M. Klumpp and A. Inayat, *Chem. Soc. Rev.*, 2016, **45**, 3353–3376.
42 M. Seifert, M. S. Marschall, T. Gille, C. Jonscher, O. Busse, S. Paasch, E. Brunner, W. Reschetilowski and J. J. Weigand, *ChemCatChem*, 2020, **12**, 6301–6310.
43 M. Seifert, M. S. Marschall, T. Gille, C. Jonscher, P. Royla, O. Busse, W. Reschetilowski and J. J. Weigand, *Chem. – Asian J.*, 2020, **15**, 3878–3885.
44 T. Zhao, F. Li, H. Yu, S. Ding, Z. Li, X. Huang, X. Li, X. Wei, Z. Wang and H. Lin, *Appl. Catal., A*, 2019, **575**, 101–110.
45 J. C. Groen, J. A. Moulijn and J. Pérez-Ramírez, *J. Mater. Chem.*, 2006, **16**, 2121–2131.
46 D. Verboekend, S. Mitchell, M. Milina, J. C. Groen and J. Pérez-Ramírez, *J. Phys. Chem. C*, 2011, **115**, 14193–14203.
47 J. C. Groen, J. A. Moulijn and J. Pérez-Ramírez, *Microporous Mesoporous Mater.*, 2005, **87**, 153–161.
48 M. Dyballa, U. Obenaus, M. Rosenberger, A. Fischer, H. Jakob, E. Klemm and M. Hunger, *Microporous Mesoporous Mater.*, 2016, **233**, 26–30.
49 K. Gao, J. Mielby and S. Kegnæs, *Catal. Today*, 2022, **405–406**, 144–151.
50 I. Pinilla-Herrero, E. Borfecchia, J. Holzinger, U. V. Mentzel, F. Joensen, K. A. Lomachenko, S. Bordiga, C. Lamberti, G. Berlier, U. Olsbye, S. Svelle, J. Skibsted and P. Beato, *J. Catal.*, 2018, **362**, 146–163.
51 Y. Yuan and R. F. Lobo, *ACS Catal.*, 2023, **13**, 4971–4984.
52 X. Su, K. Zhang, Y. Snatenkova, Z. Matieva, X. Bai, N. Kolesnichenko and W. Wu, *Fuel Process. Technol.*, 2020, **198**, 106242.
53 J. A. Biscardi, G. D. Meitzner and E. Iglesia, *J. Catal.*, 1998, **179**, 192–202.
54 E. A. Pidko and R. A. van Santen, *J. Phys. Chem. C*, 2007, **111**, 2643–2655.
55 Z. N. Lashchinskaya, A. A. Gabrienko, S. S. Arzumanov, A. A. Kolganov, A. V. Toktarev, D. Freude, J. Haase and A. G. Stepanov, *ACS Catal.*, 2020, **10**, 14224–14233.
56 M. Avramovska, D. Freude, J. Haase, A. V. Toktarev, S. S. Arzumanov, A. A. Gabrienko and A. G. Stepanov, *Phys. Chem. Chem. Phys.*, 2023, **25**, 28043–28051.
57 L. Qi, Y. Zhang, M. A. Conrad, C. K. Russell, J. Miller and A. T. Bell, *J. Am. Chem. Soc.*, 2020, **142**, 14674–14687.
58 Z. Wei, L. Chen, Q. Cao, Z. Wen, Z. Zhou, Y. Xu and X. Zhu, *Fuel Process. Technol.*, 2017, **162**, 66–77.
59 S. K. Saha and S. Sivasanker, *Catal. Lett.*, 1992, **15**, 413–418.
60 M. Dyballa, *Energy Fuels*, 2023, **37**, 18517–18559.
61 C. Rieg, Z. Li, A. Kurtz, M. Schmidt, D. Dittmann, M. Benz and M. Dyballa, *J. Phys. Chem. C*, 2020, **125**, 515–525.
62 M. Dyballa, C. Rieg, D. Dittmann, Z. Li, M. Buchmeiser, B. Plietker and M. Hunger, *Microporous Mesoporous Mater.*, 2020, **293**, 109778.
63 C. Rieg, D. Dittmann, Z. Li, R. Lawitzki, K. Gugeler, S. Maier, G. Schmitz, J. Kastner, D. P. Estes and M. Dyballa, *Chem. – Eur. J.*, 2021, **27**, 17012–17023.
64 D. Massiot, F. Fayon, M. Capron, I. King, S. Le Calvé, B. Alonso, J.-O. Durand, B. Bujoli, Z. Gan and G. Hoatson, *Magn. Reson. Chem.*, 2002, **40**, 70–76.
65 D. Müller, W. Gessner, H. J. Behrens and G. Scheler, *Chem. Phys. Lett.*, 1981, **79**, 59–62.
66 M. Müller, G. Harvey and R. Prins, *Microporous Mesoporous Mater.*, 2000, **34**, 135–147.
67 M. Dyballa, Z. Li and D. Dittmann, *Microporous Mesoporous Mater.*, 2025, **381**, 113353.
68 S. Lang, M. Benz, U. Obenaus, R. Himmelmann and M. Hunger, *ChemCatChem*, 2016, **8**, 2031–2036.
69 M. Dyballa, U. Obenaus, M. Blum and W. Dai, *Catal. Sci. Technol.*, 2018, **8**, 4440–4449.
70 M. Dyballa, D. K. Pappas, E. Borfecchia, P. Beato, U. Olsbye, K. P. Lillerud, B. Arstad and S. Svelle, *Microporous Mesoporous Mater.*, 2018, **265**, 112–122.
71 H. G. Karge, M. Lsaniecki, M. Ziolek, G. Onyestyák, A. Kiss, P. Kleinschmit and M. Siray, in *Zeolites: Facts, Figures, Future Part A - Proceedings of the 8th International Zeolite Conference*, ed. P. A. Jacobs and R. A. van Santen, Studies in Surface Science and Catalysis, Elsevier, Amsterdam, 1989, vol. 49B, pp. 1327–1337.
72 J. Goetze, F. Meirer, I. Yarulina, J. Gascon, F. Kapteijn, J. Ruiz-Martínez and B. M. Weckhuysen, *ACS Catal.*, 2017, **7**, 4033–4046.
73 N. C. Deno, J. Bollinger, N. Friedman, K. Hafer, J. D. Hodge and J. J. Houser, *J. Am. Chem. Soc.*, 1963, **85**, 2998–3000.
74 W. Dai, C. Wang, M. Dyballa, G. Wu, N. Guan, L. Li, Z. Xie and M. Hunger, *ACS Catal.*, 2014, **5**, 317–326.
75 M. Bjørgen, F. Bonino, S. Kolboe, K.-P. Lillerud, A. Zecchina and S. Bordiga, *J. Am. Chem. Soc.*, 2003, **125**, 15863–15868.
76 Y. Jiang, J. Huang, J. Weitkamp and M. Hunger, in *Studies in Surface Science and Catalysis*, ed. R. Xu, Z. Gao, J. Chen and W. Yan, Elsevier, 2007, vol. 170, pp. 1137–1144.
77 R. Liu, X. Shao, C. Wang, W. Dai and N. Guan, *Chin. J. Catal.*, 2023, **47**, 67–92.